Low-Complexity Adaptive Beamforming Algorithm With High Dimensional and Small Samples

Xuejun Zhang and Dazheng Feng, *Member, IEEE*

***Abstract*—A large-scale array (LSA) inevitably encounters scenarios with a small number of samples, and its beamformer suffers from high computational complexity. High computational complexity prevents the system from being used in practical online engineering applications. The complex vector of the beamformer weights can be expressed as the product of training snapshots and the signal steering vector (SSV), and a coefficient vector, since the optimal weight vector is a linear combination of basis vectors of the signal-plus-interference subspace. In this study, a new adaptive beamformer is developed based on the minimum variance distortionless response (MVDR) criterion and kernel techniques. The new beamformer only needs to compute the inversion of a low-dimensional Gram matrix instead of the high-dimensional sample covariance matrix (SCM), which significantly reduces the calculation cost. Moreover, an efficient loading parameter calculation method (only related to the received matrix and not required user-defined parameters) is derived, which can adaptively suppress the mismatches of the ill-conditioned Gram matrix. Furthermore, a fast version of the new beamformer is formulated for the LSA under the scanning mode. Simulation results demonstrate that the new beamformer achieves better performance and a lower computation load than existing algorithms for a small number of samples. In particular, insufficient samples and high computational complexity problems are more frequently aroused in space-time broadband array signal processing. Interestingly, the new techniques can be successfully extended to wideband array signal processing and yield satisfactory beam pattern shapes.**

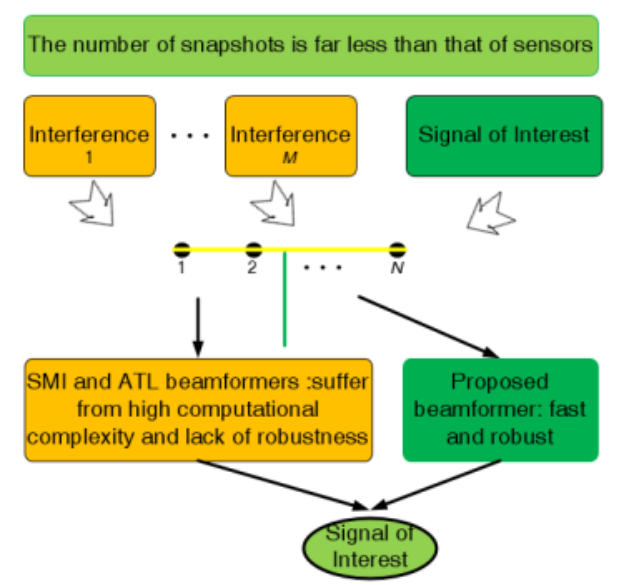

***Index Terms*—Gram matrix, large-scale array (LSA), sample covariance matrix (SCM), scanning mode, shrinkage technique, small samples case, wideband beamforming.**

I. Introduction

ADAPTIVE array processing has been widely adopted in wireless communications, medical imaging, radar [1], [3], [5], [8], [22], [27], [29], [31], [33], [52], sonar [4], radio astronomy [6], seismology, microphone array speech processing [7], [32], and other areas. To achieve superior performance, an increasing number of sensors are being configured in modern array systems [33], [35]. Hence, to achieve acceptable performance (within 3 dB of the optimal value) [1], the number of homogeneous snapshots required is also increasing. It should be noted that this essential requirement is difficult to meet in actual applications, especially in the case of space-heterogeneous and time-changeable external interferences and white noise [2]. Moreover, in this scenario, high calculation costs prevent the use of robust adaptive beamforming (RAB) algorithms in online processing. Furthermore, the number of modern system sensors is frequently and significantly greater than that of usable and independent, and identically distributed snapshots, which makes several

Manuscript received 15 January 2023; accepted 13 February 2023. Date of publication 27 March 2023; date of current version 14 July 2023. This work was supported in part by the National Natural Science Foundation of China under Grant 61971470 and Grant 61971349. The associate editor coordinating the review of this article and approving it for publication was Dr. Priyadip Ray. *(Corresponding author: Dazheng Feng.)*

The authors are with the National Key Laboratory of Radar Signal Processing, Xidian University, Xi'an 710071, China (e-mail: zhangxuejun@stu.xidian.edu.cn; dzfeng@xidian.edu.cn).

Digital Object Identifier 10.1109/JSEN.2023.3250265

RAB algorithms invalid. In fact, the problems of insufficient samples and big computation load also frequently appear in the multiple–input-multiple–output (MIMO) radars [10], [11], [12], [29], [34] and the space-time broadband array signal processing systems [30], [32], where the degrees of freedom are usually much greater than the number of external interference and the clutter subspace. Therefore, rapid convergence and low calculation cost are critical requirements for modern array systems [1], [34], [35].

Many RAB algorithms [1], [3], [4], [5], [9], [10], [11], [12], [13], [14], [16], [17], [18], [19], [20], [21], [22], [49], [50], [51], [52] have been proposed in previous decades. The most well-known one is the quadratically constrained beamformer, which is also called the loaded sample matrix inversion (LSMI) beamformer [whose implementation is based on diagonal loading [14], [15], [30], [31], [43], [44] of the sample covariance matrix (SCM)]. The LSMI beamformer, whose convergence rate is higher than that of the sample matrix inversion (SMI) beamformer, can efficiently deal with arbitrary mismatches [17] (e.g., mismatches caused by array perturbations, array manifold mismodeling, wavefront distortions, frequency mismatch, and source local scattering). Compared with the LSMI beamformer, the beamformer proposed in [43] exhibits several remarkable advantages, such as high convergence rate and low calculation cost. The RAB algorithm proposed in [17] is a type of diagonal loading approach, where the diagonal loading level is determined by the uncertainty set of the signal steering vector (SSV), which is based on the worst case performance optimization (WCPO) criteria. Hence, we need to specify the parameter related to the size of the uncertainty set, and this approach involves repeated optimization and high calculation costs. The well-known eigenspace-based algorithms [18], [51], [52] aim to eliminate the covariance matrix uncertainty [45], [48]. In [50], a novel subspace method (a kind of covariance matrix reconstruction (CMR) beamformer) is proposed to reconstruct the interference-plus-noise covariance matrix according to its definition, which can fundamentally eliminate the signal-of-interest (SOI) component from the SCM. Their main idea [18], [51], [52] is to employ the accurately estimated independent interference SSV [45], [48] to build an improved covariance matrix and to achieve robustness against various types of model mismatches. It is well known that, especially in significant noise cases, determining the number of sources is a challenge in practical applications [45], [48]. The most frequently used methods [19] are the Akaike information criterion and Rissanen's minimum description length principle, which refer to the information theory criteria. All these techniques [19] are strongly dependent on the separability of the eigenvalues of the array covariance matrix. Hence, these algorithms usually fail when the signal-to-noise ratio (SNR) is low or the number of snapshots is insufficient. Although RAB algorithms [11], [45], [48], [51], [52] can deal with arbitrary model errors, the convergence measures of effectiveness (MOEs) [1] of these beamformers [14], [15], [30], [31], [43], [44] are approximately twice the number of external interferences. Moreover, the high calculation cost of these beamformers [33], [35] prevents their use in real-time applications.

Several RAB approaches [12], [21] with reduced dimension or rank have also been proposed. These algorithms [12], [21] have a high convergence rate and low computational cost. The most well-known one is the multistage Wiener filter (MSWF), which is an alternative form of the conjugate gradient (CG) algorithm. The auxiliary-vector filtering (AVF) algorithm is another efficient RAB algorithm, which is similar to MSWF. It iteratively updates the weight vector, which is initialized by the conjugated SSV. In [53], a generalized reduced-rank structure is established for the broadband space-time GSC. The generalized structure estimates signal subspace by a reduced-rank transform matrix, so the dimension of the broadband signal data vector is decreased. It is worth noting that MSWF, CG, AVF, and [53] are equipped with the same range, which is called the Krylov subspace [21]. In most cases (correct model rank), array signal processing tasks (such as estimating the direction of arrival, suppressing interference and noise, and beamforming) are effectively handled by these approaches [1], [12], [21], [45], [48]. It has been known that these algorithms [1], [12], [21], [45], [48] not only require prior information regarding the external interferences and order of the signal model but also are highly sensitive to slight mismatches caused by the model order estimation.

The beam synthesizer and partially adaptive beamformer [12], [21], [26], [27] have a low calculation cost and do not require sufficient training snapshots. Moreover, there is phase wrapping between the subarrays. The performance of the beam synthesizer will be severely degraded because of the grating lobes. Recently, factorized methods [12], [21] with reduced rank have attracted considerable attention. The optimal factorized approach proposed in [12] has two important advantages: 1) the large-scale array (LSA) is equipped with highly redundant degrees of freedom and 2) the optimal complex vector of the beamformer weight lies in a low-dimensional subspace (signal-plus-interference subspace). Due to these advantages, reduced-rank approaches [12], [21] are highly effective.

This study develops an RAB algorithm with high convergence rate and low computational cost for LSA with a small number of samples. The weight vector of the beamformer is formulated as a linear combination of training snapshots and the presumed SSV. The proposed algorithm only needs to compute the inversion of a low-dimensional Gram matrix instead of the high-dimensional SCM, which significantly reduces the computational complexity. Furthermore, an efficient loading-level calculation method is proposed, which can adaptively suppress the random variation caused by the presence of mismatches of the ill-conditioned Gram matrix. Also, the loading-level calculation method does not require prior knowledge (such as the number of interferences, the user-defined parameters, and the level of noise). Moreover, a scanning version of the new beamformer with low computational complexity is developed, as the loading factor is only determined by the received matrix. Simulation results confirm that the proposed algorithm achieves good performance and high efficiency for a small number of samples. In addition, the proposed algorithm is successfully applied to broadband array signal processing (space-time and

subband techniques) and obtains a satisfactory beam pattern shape.

The remainder of this article is organized as follows. Section II presents background information on the beamformer weight vector. Section III describes the proposed RAB algorithm in detail and analyzes the regularization technique. Section IV presents the experimental results. Finally, Section V concludes this article.

Notations: In the article, boldface capital letters and lower case letters denote matrices and vectors, respectively. Given a matrix $\mathbf{A}$, the symbols $\mathbf{A}^*$, $\mathbf{A}^H$, $\mathbf{A}^{-1}$, and $\mathbf{A}^+$ denote the complex conjugate, Hermitian transpose, inverse, and Moore–Penrose inverse of $\mathbf{A}$, respectively; and $\mathbf{I}_N$ denotes an $N \times N$ identity matrix Furthermore, $E\{\bullet\}$ denotes the expectation operator, $\otimes$ is the Kronecker product, $\odot$ is the entry-wise product, $\lfloor \bullet \rfloor$ denotes the ceil operator, trace$\{\bullet\}$ denotes the operation of matrix trace, $\| \bullet \|$ denotes the Forbenius norm of a matrix or the Euclidean norm of a vector, $\mathbb{C}$ denotes the complex set, and σ_n^2 denotes the noise power.

II. Problem Formulation

For simplicity and without loss of generality, consider a uniform linear array (ULA) comprising N sensors and a cluster of $M + 1$ far-field narrowband point signals (i.e., an expected signal and M external interference sources) impinging on the array simultaneously (as shown in Fig. 1).

The received data vector is given by the following equation:

$$\begin{aligned}\mathbf{x}(l) &= s_s(l)\,\mathbf{a}(\theta_s) + \sum_{m=1}^{M} s_m(l)\,\mathbf{a}(\theta_m) + \mathbf{n}(l) \\ &= \mathbf{A}\mathbf{s}(l) + \mathbf{n}(l)\end{aligned} \tag{1}$$

where l is the snapshot index. Here, $s_s(l)$ and $s_m(l), m = 1, 2, \ldots, M$, is the complex amplitude of the signal and interferences, respectively. Let $\mathbf{a}(\theta) \in \mathbb{C}^{N\times 1}$ represent the spatial signature (or SSV) in the direction of θ, $\mathbf{A} = [\mathbf{a}(\theta_s), \mathbf{a}(\theta_1), \ldots, \mathbf{a}(\theta_M)] \in \mathbb{C}^{N\times(M+1)}$ denote the signal and interferences array manifold matrix, and $\mathbf{s}(l) \in \mathbb{C}^{(M+1)\times 1}$ represent the complex amplitude response vector. Furthermore, let the noise vector $\mathbf{n}(l) \in \mathbb{C}^{N\times 1}$ denote complex Gaussian white noise (we assume that the signal, interferences, and noise are mutually independent of each other).

Remark 1: Suppose that the scale of ULA is so large that the numbers of interferences and snapshots are far smaller than the number of sensors. In many real-time MIMO applications, the number of sensors sometimes exceeds 10 000, and the number of snapshots varies from tens to hundreds. Also, in the wideband array signal processing area, the scale of space-time structure may be much greater than the number of useable and independent, and identically distributed training samples.

Based on the minimum variance distortionless response (MVDR) criterion [1], [24], we get the following expression:

$$\begin{cases} \underset{\mathbf{w}}{\text{minimize}} & \mathbf{w}^H\mathbf{R}_{i+n}\mathbf{w} \\ \text{subject to} & \mathbf{w}^H\mathbf{a} = 1 \end{cases} \tag{2}$$

where $\mathbf{R}_{i+n} = E\{(\mathbf{i}(l) + \mathbf{n}(l))(\mathbf{i}(l) + \mathbf{n}(l))^H\} \in \mathbb{C}^{N\times N}$ is the exact interference-plus-noise covariance matrix. The optimal weight vector of the MVDR beamformer is easily obtained as follows:

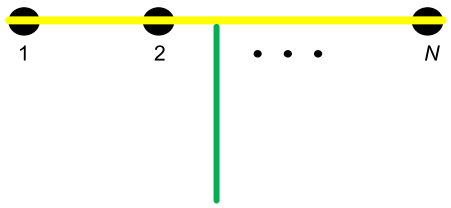

Fig. 1. Coordinates of ULA.

$$\mathbf{w}_{\text{opt}} = \lambda\mathbf{R}_{i+n}^{-1}\mathbf{a} \tag{3}$$

where $\lambda = (\mathbf{a}^H\mathbf{R}_{i+n}^{-1}\mathbf{a})^{-1}$ is a normalization constant [17], [43]. In general, the ideal interference-plus-noise covariance matrix can be decomposed into the following two parts:

$$\mathbf{R}_{i+n} = \mathbf{R}_i + \mathbf{R}_n \tag{4}$$

where $\mathbf{R}_i \in \mathbb{C}^{N\times N}$ and $\mathbf{R}_n \in \mathbb{C}^{N\times N}$ denote the interference and noise covariance matrices, respectively. It is reasonable to assume that $\mathbf{R}_n = \sigma_n^2\mathbf{I}_N$ under complex Gaussian white noise.

The eigenvalue decomposition (EVD) of $\mathbf{R}_i$ is written as follows:

$$\mathbf{R}_i = \mathbf{U}_i\mathbf{\Lambda}_i\mathbf{U}_i^H \tag{5}$$

where $\mathbf{\Lambda}_i \in \mathbb{C}^{M\times M}$ denotes a diagonal matrix whose diagonal elements are the eigenvalues of $\mathbf{R}_i$ and $\mathbf{U}_i \in \mathbb{C}^{N\times M}$ consists of eigenvectors corresponding to the non-zero eigenvalues of the interference covariance matrix. By substituting (4) and (5) into (3) and using the matrix inversion lemma, we have the following expression:

$$\begin{aligned}\tilde{\mathbf{w}}_{\text{opt}} &= \mathbf{R}_n^{-1}\mathbf{a} - \mathbf{R}_n^{-1}\mathbf{U}_i\left(\mathbf{U}_i^H\mathbf{R}_n^{-1}\mathbf{U}_i + \mathbf{\Lambda}_i^{-1}\right)^{-1}\mathbf{U}_i^H\mathbf{R}_n^{-1}\mathbf{a} \\ &= \sigma_n^{-2}\mathbf{a} - \sigma_n^{-4}\mathbf{U}_i\left(\sigma_n^{-2}\mathbf{I}_M + \mathbf{\Lambda}_i^{-1}\right)^{-1}\mathbf{U}_i^H\mathbf{a} \\ &= [\mathbf{a}, \mathbf{U}_i]\left[\sigma_n^{-2}; -\sigma_n^{-4}\left(\sigma_n^{-2}\mathbf{I}_M + \mathbf{\Lambda}_i^{-1}\right)^{-1}\mathbf{U}_i^H\mathbf{a}\right].\end{aligned} \tag{6}$$

Here, we define

$$\mathbf{c} = \left[\sigma_n^{-2}; -\sigma_n^{-4}\left(\sigma_n^{-2}\mathbf{I}_M + \mathbf{\Lambda}_i^{-1}\right)^{-1}\mathbf{U}_i^H\mathbf{a}\right]. \tag{7}$$

Obviously, (6) suggests that the optimal weight vector is located in the subspace, which is spanned by the SSV and interference steering vectors (signal-plus-interference subspace). Obtaining the complete signal-plus-interference subspace is the primary task of the study. However, $\mathbf{R}_{i+n}$ is unavailable [43], [45], [48]. We employ the SCM instead of the ideal interference-plus-noise covariance matrix to estimate the signal-plus-interference subspace

$$\begin{aligned}\hat{\mathbf{R}} &= \frac{1}{L}\sum_{l=1}^{L}\mathbf{x}(l)\,\mathbf{x}^H(l) \\ &= \frac{1}{L}\mathbf{X}\mathbf{X}^H\end{aligned} \tag{8}$$

where L is the number of snapshots, $\mathbf{X} = [\mathbf{x}(1), \ldots, \mathbf{x}(L)]$.

Assume that the number of snapshots is smaller than that of sensors; then, $\hat{\mathbf{R}} \in \mathbb{C}^{N\times N}$ is substantially underestimated, as in the case of a small number of samples [1]. Hence, the obtained signal-plus-interference subspace may be incomplete. Moreover, the sensor array scale is so large that calculating the signal-plus-interference subspace involves high computational costs. However, the received data vectors contain numerous expected signal and interference components when the SNR is sufficiently high. When the SNR is low, the desired SSV is weak; we append the presumed SSV to the data vectors and build a complete signal-plus-interference subspace.

III. Adaptive Beamforming and Fast Version

A. MVDR Beamformer

From (6), the optimal weight vector is expressed as the product between a linear combination and the basis vectors of the signal-plus-interference subspace. It is easily seen that the range of the data matrix contains the interference subspace. However, the desired signal components may not be present in the data matrix. Hence, we use the data matrix and presumed SSV to construct the signal-plus-interference subspace. According to the MVDR criterion [17], [43], the new beamforming optimization problem is formulated as follows:

$$\begin{cases} \underset{\boldsymbol{\beta}}{\text{minimize}} & \mathbf{w}^H \hat{\mathbf{R}} \mathbf{w} \\ \text{subject to} & \widehat{\mathbf{X}} = [\mathbf{a}, \mathbf{X}], \ \mathbf{w} = \widehat{\mathbf{X}}\boldsymbol{\beta}, \ \mathbf{w}^H\mathbf{a} = 1 \end{cases} \tag{9}$$

where $\boldsymbol{\beta}$ denotes the linear combination vector. Using the Lagrange multiplier method, we transform (9) into an unconstrained quadratic optimization problem. Hence, we have

$$\underset{\boldsymbol{\beta},\hat{\lambda}}{\text{minimize}} \left(\widehat{\mathbf{X}}\boldsymbol{\beta}\right)^H \hat{\mathbf{R}} \left(\widehat{\mathbf{X}}\boldsymbol{\beta}\right) + \hat{\lambda}\left(\boldsymbol{\beta}^H \widehat{\mathbf{X}}^H \mathbf{a} - 1\right) \tag{10}$$

where $\hat{\lambda}$ denotes the Lagrange multiplier factor. Calculating the gradient of (10) with respect to $\boldsymbol{\beta}^H$ and letting it equal to zero vector, we get the following equation:

$$\widehat{\mathbf{X}}^H \hat{\mathbf{R}} \left(\widehat{\mathbf{X}}\boldsymbol{\beta}\right) + \hat{\lambda}\widehat{\mathbf{X}}^H \mathbf{a} = \mathbf{0}. \tag{11}$$

According to $\mathbf{w}^H\mathbf{a} = 1$, we have

$$\hat{\lambda} = \frac{-1}{\mathbf{a}^H \widehat{\mathbf{X}} \left(\widehat{\mathbf{X}}^H \hat{\mathbf{R}} \widehat{\mathbf{X}}\right)^+ \widehat{\mathbf{X}}^H \mathbf{a}}. \tag{12}$$

From the relation given by (11) and (12), the linear combination vector is calculated as follows:

$$\boldsymbol{\beta}_{\text{MVDR}} = \frac{\left(\widehat{\mathbf{X}}^H \hat{\mathbf{R}} \widehat{\mathbf{X}}\right)^+ \widehat{\mathbf{X}}^H \mathbf{a}}{\mathbf{a}^H \widehat{\mathbf{X}} \left(\widehat{\mathbf{X}}^H \hat{\mathbf{R}} \widehat{\mathbf{X}}\right)^+ \widehat{\mathbf{X}}^H \mathbf{a}}. \tag{13}$$

By applying (9)–(13), the proposed beamformer is derived as follows:

$$\begin{aligned} \tilde{\mathbf{w}}_{\text{MVDR}} &= \widehat{\mathbf{X}}\beta_{\text{MVDR}} \\ &= \frac{[\mathbf{a}, \mathbf{X}]\left([\mathbf{X}^H\mathbf{a}, \mathbf{X}^H\mathbf{X}]^H [\mathbf{X}^H\mathbf{a}, \mathbf{X}^H\mathbf{X}]\right)^+ [\mathbf{a}, \mathbf{X}]^H \mathbf{a}}{\mathbf{a}^H [\mathbf{a}, \mathbf{X}]\left([\mathbf{X}^H\mathbf{a}, \mathbf{X}^H\mathbf{X}]^H [\mathbf{X}^H\mathbf{a}, \mathbf{X}^H\mathbf{X}]\right)^+ [\mathbf{a}, \mathbf{X}]^H \mathbf{a}}. \end{aligned} \tag{14}$$

Let $\widehat{\mathbf{R}} \in \mathbb{C}^{L\times L}$ represent the Gram matrix (linear kernel matrix) [28], which is given by the following equation:

$$\widehat{\mathbf{R}} = \frac{\mathbf{X}^H\mathbf{X}}{N}. \tag{15}$$

It is easy to prove that $\widehat{\mathbf{R}}$ is a positive definite matrix. Therefore, the relation given by (14) is rewritten in the following form:

$$\begin{aligned} \tilde{\mathbf{w}}_{\text{MVDR}} &= \widehat{\mathbf{X}}\boldsymbol{\beta}_{\text{MVDR}} \\ &= \frac{[\mathbf{a}, \mathbf{X}]\left(\left[\mathbf{X}^H\mathbf{a}, N\widehat{\mathbf{R}}\right]^H \left[\mathbf{X}^H\mathbf{a}, N\widehat{\mathbf{R}}\right]\right)^+ [\mathbf{a}, \mathbf{X}]^H \mathbf{a}}{\mathbf{a}^H [\mathbf{a}, \mathbf{X}]\left(\left[\mathbf{X}^H\mathbf{a}, N\widehat{\mathbf{R}}\right]^H \left[\mathbf{X}^H\mathbf{a}, N\widehat{\mathbf{R}}\right]\right)^+ [\mathbf{a}, \mathbf{X}]^H \mathbf{a}} \end{aligned} \tag{16}$$

and $\hat{\lambda} = 1/(\mathbf{a}^H[\mathbf{a}, \mathbf{X}]([\mathbf{X}^H\mathbf{a}, N\widehat{\mathbf{R}}]^H[\mathbf{X}^H\mathbf{a}, N\widehat{\mathbf{R}}])^+[\mathbf{a}, \mathbf{X}]^H\mathbf{a})$ is a normalization constant, which does not affect the output signal-to-interference-plus-noise ratio (SINR). Hence, $\hat{\lambda}$ is omitted as usual. Also, (16) is further simplified into the following expression:

$$\begin{aligned} \mathbf{w}_{\text{MVDR}} &= \widehat{\mathbf{X}}\tilde{\boldsymbol{\beta}} \\ &= [\mathbf{a}, \mathbf{X}]\left(\left[\mathbf{X}^H\mathbf{a}, N\widehat{\mathbf{R}}\right]^H \left[\mathbf{X}^H\mathbf{a}, N\widehat{\mathbf{R}}\right]\right)^+ [\mathbf{a}, \mathbf{X}]^H \mathbf{a}. \end{aligned} \tag{17}$$

Although the linear kernel matrix $\widehat{\mathbf{R}}$ is a positive definite matrix, it is an ill-conditioned matrix for a small number of training samples. For the ill-posed Gram matrix $\widehat{\mathbf{R}}$, the ratio of its smallest eigenvalue to its largest eigenvalue is close to zero. Specifically, the linear combination vector is determined by the high-frequency (smallest eigenvalue) components of the Gram matrix [28], which corresponds to the model mismatches (including noise and errors). Consequently, the linear combination vector is often random, and the beamformer achieves poor performance.

It is well known that the regularization technique can be considered as a type of low-pass filtering technique [1], [43] that can efficiently suppress the high-frequency components of the Gram matrix. In Section III-B, the diagonal loading technique (based on the shrinkage technique) is adopted to deal with the ill-posed problem caused by an ill-conditioned Gram matrix.

B. Proposed Beamformer Based on Loading Technique

The regularization technique is the most efficient way to deal with the ill-conditioned problem [43]. Diagonal loading [14], [15], [30], [31], [43], [44] is a well-known robust technique, which is also called norm constraint regularization [43]. The main drawback of this method is that there is no analytical way to reliably determine the optimal diagonal loading level.

Our main motivations for the use of the shrinkage technique areas are given as follows. The shrinkage technique (computationally simple and fully automatic method [2]) is a kind of norm constraint regularization, which can efficiently suppress model mismatches. Hence, we adopt shrinkage-based [2] Gram matrix estimation instead of the sample Gram matrix

in the standard MVDR beamforming formulation. Also, the shrinkage technique does not require user-defined parameters (prior knowledge). Therefore, the loading factor calculation method computes the loading level in a fully automatic manner from the received data.

Considering a more general linear combination (GLC) [2], the improved Gram matrix has the following form:

$$\tilde{\mathbf{R}} = \alpha \mathbf{I}_L + \kappa \widehat{\mathbf{R}} \tag{18}$$

where $\alpha \geq 0$ and $\kappa \geq 0$ are the shrinkage parameters (a kind of loading factor) for the GLC. The parameters can be obtained by minimizing the mean square error (MSE) of the estimator $\tilde{\mathbf{R}} \in \mathbb{C}^{L\times L}$, where $\mathrm{MSE}(\tilde{\mathbf{R}}) = \mathrm{E}\{\|\tilde{\mathbf{R}} - \bar{\mathbf{R}}\|\}$. Here, $\bar{\mathbf{R}}$ denotes the ideal Gram matrix.

Let $\mathbf{Z} = \mathbf{X}^H \in \mathbb{C}^{L\times N}$ denote the conjugate transpose of the data matrix. To estimate α and κ from the received data, we need an estimate of ρ, which is given by (see [2] for further details)

$$\rho = \frac{1}{N^2}\sum_{n=1}^{N} \|\mathbf{z}_n\|^4 - \frac{1}{N}\|\widehat{\mathbf{R}}\|^2 \tag{19}$$

where $\mathbf{z}_n$ denotes the nth column of $\mathbf{Z}$. Similarly, we can get the estimates of γ and ν, which are given by the following equation:

$$\nu = \mathrm{trace}\left(\widehat{\mathbf{R}}\right) \tag{20}$$

$$\gamma = \|\nu \mathbf{I}_L - \widehat{\mathbf{R}}\|^2. \tag{21}$$

Then, α and κ are calculated as follows:

$$\alpha = \frac{\gamma}{\gamma + \rho} \tag{22}$$

$$\kappa = \nu\,(1-\alpha)\,. \tag{23}$$

By applying (21) and (22) to (17), the beamformer based on the shrinkage technique is formulated as follows:

$$\mathbf{w}_{\mathrm{LT}} = [\mathbf{a}, \mathbf{X}]\left(\left[\mathbf{X}^H\mathbf{a}, N\tilde{\mathbf{R}}\right]^H\left[\mathbf{X}^H\mathbf{a}, N\tilde{\mathbf{R}}\right]\right)^{+}[\mathbf{a}, \mathbf{X}]^H\,\mathbf{a}. \tag{24}$$

C. Fast Version of Beamformer Weight Vector

The adaptive beamforming algorithm frequently works in the scanning mode. In this scenario, the weight vector of the proposed beamformer must be repeatedly calculated for different directions. Let $\{\hat{\theta}\}_{\hat{k}=1}^{\hat{K}}$ be a fixed sampling grid that uniformly covers the angle range $[-\pi/2, \pi/2]$, where $\hat{K}$ denotes the grid number. Similarly, let $\{\bar{\theta}\}_{\bar{k}=1}^{\bar{K}}$ be a grid that nonuniformly covers the angle range (number of signals), where $\bar{K}$ is the number of presumed SSVs. Hence, the beampattern is given by the following equation:

$$\widehat{f} = |\mathbf{a}^H\left(\hat{\theta}\right)\mathbf{w}_{\mathrm{LT}}\left(\bar{\theta}\right)|. \tag{25}$$

Let $\mathbf{b} = \mathbf{X}^H\mathbf{a}(\bar{\theta}_{\bar{k}})$, $\widehat{\mathbf{R}}_1 = N(\alpha\mathbf{I}_L + \kappa\widehat{\mathbf{R}})$, and $\mathbf{c} = [\mathbf{a}^H(\bar{\theta}_{\bar{k}})\mathbf{a}(\bar{\theta}_{\bar{k}}); \mathbf{b}]$. Hence, the fast version of the proposed beamformer is given by the following equation:

$$\mathbf{w}_{\mathrm{LT}} = \left[\mathbf{a}\left(\bar{\theta}_{\bar{k}}\right), \mathbf{X}\right]\left(\left(\left[\mathbf{b}, \widehat{\mathbf{R}}_1\right]^H\left[\mathbf{b}, \widehat{\mathbf{R}}_1\right]\right)^{+}\mathbf{c}\right). \tag{26}$$

Here, the fast form of the beamformer given by (26) has been presented such that $\mathbf{w}_{\mathrm{LT}}(\bar{\theta}_{\bar{k}})$ can be a fast update for each direction during the beam scanning processing.

TABLE I
STEPS OF THE PROPOSED BEAMFORMING ALGORITHM

Proposed Beamforming Algorithm
Objective: Calculate the weight vector of the proposed algorithm.
Input: Give received data matrix $\mathbf{X}$ and presumed SSV $\mathbf{a}$.
1) Obtain $\tilde{\mathbf{R}}=\left(\mathbf{X}^{\mathrm{H}}\mathbf{X}\right)/N$
2)Calculate $\alpha=\gamma/(\gamma+\rho)$, $\kappa=\nu(1-\alpha)$ by employing $\rho=\frac{1}{N^2}\left(\sum_{n=1}^{N}\|\mathbf{z}_n\|^4\right)-\frac{1}{N}\|\widehat{\mathbf{R}}\|^2$, $\nu=\mathrm{trace}\left(\tilde{\mathbf{R}}\right)$, $\gamma=\|\nu\mathbf{I}_L-\widehat{\mathbf{R}}\|^2$.
3) Compute $\mathbf{b}=\mathbf{X}^{\mathrm{H}}\mathbf{a}$, $\widehat{\mathbf{R}}_1=N\left(\alpha\mathbf{I}_L+\kappa\widehat{\mathbf{R}}\right)$, $\mathbf{c}=\left[\mathbf{a}^{\mathrm{H}}\mathbf{a};\mathbf{b}\right]$.
4) Determine the weight vector of the proposed algorithm $\mathbf{w}_{\mathrm{LT}}$ by using $[\mathbf{a},\mathbf{X}]\left(\left[\mathbf{b},\widehat{\mathbf{R}}_1\right]^{\mathrm{H}}\left[\mathbf{b},\widehat{\mathbf{R}}_1\right]\right)^{\dagger}\mathbf{c}$.
5) Get $\mathbf{w}_{\mathrm{LT}}$.

Table I shows the pseudocode of the fast version of the proposed algorithm.

D. Version of Wideband Beamforming

Broadband beamforming has attracted increased attention over the past few decades because of its extensive applications in various fields. It is a well-known fact that wideband beamforming can be generally categorized into two parts: space-time beamforming and subband beamforming.

Subband beamforming algorithms mainly include two substeps: 1) decomposes the received wideband signal into multiple frequency bins and 2) employs the narrowband beamforming techniques, at each frequency bin. Thus, our algorithm can process the narrowband signal. It can be seen that (16) is a kind of subband beamforming algorithm.

Here, a new space-time beamformer is proposed by applying the Frost filter structure, which accomplishes the broadband adaptive beamforming algorithm based on the MVDR. Table II descries the pseudo algorithm of the new space-time technique (see the Appendix for further details).

E. Analysis of Computational Complexity of the Proposed Beamformer

In this section, we discuss the computational complexity of both the proposed algorithm and classical low-computational-complexity beamformers (such as the LSMI and ATL beamformers), and we will only retain the highest order of computational complexity. The computational complexity of a beamformer depends on its working mode. The loading factor of the LSMI beamformer does not depend on the presumed SSV. Here, Gaussian elimination methods are used to perform the inversion operation, in which computational

TABLE II
STEPS OF THE PROPOSED SPACE-TIME BEAMFORMING ALGORITHM

Space-Time Beamforming Algorithm
Objective: Compute the space-time weight vector.
Input: Provide the received date $\mathbf{X}_1$, and the presumed direction of arrival (DOA) θ.
1) The frequency band is decomposed into P bins $f_i, i = 1, 2, \mathrm{L}, P$.
2) Obtain the frequency domain constraint matrix $\mathbf{C}_{\mathrm{F}} = [\mathbf{c}_{\mathrm{F}}(f_1), \mathbf{c}_{\mathrm{F}}(f_2), \mathrm{L}, \mathbf{c}_{\mathrm{F}}(f_J)] \in \pounds^{NP \times P}$.
3) Calculate the well-known space-time response vector $\mathbf{f}_d = \left[e^{-j2\pi f_1(P-1)/2}, e^{-j2\pi f_2(P-1)/2}, \mathrm{L}, e^{-j2\pi f_J(P-1)/2}\right]^{\mathrm{T}}$.
4) Compute $\mathbf{R}_2 = \mathbf{X}_1^{\mathrm{H}}\mathbf{X}_1$, $\mathbf{R}_3 = \mathbf{X}_1^{\mathrm{H}}\mathbf{C}_{\mathrm{F}}(\theta)$, $\mathbf{R}_5 = [\mathbf{C}_2, \mathbf{R}_3^{\mathrm{H}}]$, $\mathbf{C}_2 = \mathbf{C}_{\mathrm{F}}^{\mathrm{H}}\mathbf{C}_{\mathrm{F}}$, $\mathbf{R}_4 = \left([\mathbf{R}_3, \mathbf{R}_2]^{\mathrm{H}}[\mathbf{R}_3, \mathbf{R}_2]\right)/L_3$.
5) Obtain: $\mathbf{W}_{\mathrm{ST}} = [\mathbf{C}_F, \mathbf{X}_1]\mathbf{R}_4^{-1}\mathbf{R}_5^{\mathrm{H}}\left(\mathbf{R}_5\mathbf{R}_4^{-1}\mathbf{R}_5^{\mathrm{H}}\right)^{-1}\mathrm{diag}(\mathbf{f}_d)$
6) Get $\mathbf{W}_{\mathrm{ST}}$.

complexity is $2N^3/3$ flops. The computational complexity of EVD of the SCM takes approximately $4N^3$ flops, if the EVD is performed by the Jacobian transform. It should be pointed out that matrix inversion and EVD are difficult to be implemented by parallel processing unlike the matrix multiplication. This shows that the inversion and the EVD of the SCM are two computational obstacles for various beamformers.

It is easy to count that the computational complexity of the LSMI beamformer is about $N^2L + 14N^3/3$ flops, where a flop [43] is a floating-point multiplication. In contrast, the loading parameters of the ATL beamformer are associated with the presumed SSV in each case. Therefore, the total computational complexity of the ATL beamforming algorithm is approximately $N^2L + 2N^3/3$ flops.

As shown in (24), the computational complexity of the fast version consists of several common parts. Calculating loading parameters requires $NL + 2L^2 + N + L$ flops. Constructing the matrix $\bar{\mathbf{R}}_3 = [\mathbf{X}^H\mathbf{a}, N(\alpha\mathbf{I}_L + \kappa\widehat{\mathbf{R}})] = [\mathbf{X}^H\mathbf{a}, N(\alpha\mathbf{I}_L + (\kappa)/(N)\mathbf{X}^H\mathbf{X})]$ requires $NL(L+1) + L(L+1)$ flops. Calculating $\mathbf{c}_1 = [\mathbf{a}, \mathbf{X}]^H\mathbf{a} \in \mathbb{C}^{(L+1)\times 1}$ needs $(L+1)N$ flops. Calculating $\mathbf{R}_3 = \bar{\mathbf{R}}_3^H\bar{\mathbf{R}}_3 \in \mathbb{C}^{(L+1)\times(L+1)}$ and its pseudoinversion requires $(L+1)^2L$ and $(2)/(3)(L+1)^3$ flops, respectively. Computing $\mathbf{c}_2 = \mathbf{R}_3^+\mathbf{c}_1 \in \mathbb{C}^{(L+1)\times 1}$ takes $(L+1)^2$ flops. Processing $\mathbf{c}_3 = [\mathbf{a}, \bar{\mathbf{X}}]\mathbf{c}_2$ needs $(L+1)N$ flops. Performing normalization constant requires $L+2$ flops. It can be seen that the computational complexity of building the weight vector is approximately equal to $5(L+1)^3/3 + N(L+1)^2$ flops (the lower order terms are omitted in this case).

The number of sensors (e.g., 500) is much larger than that of samples (for instance, 50) in a modern array system. Hence, the computational complexity of the proposed algorithm is much lower than that of the LSMI [14], [15], [30], [31] and ATL [43] beamformers for high-dimensional data in the case of small samples. Thus, the proposed narrowband beamformer may be better suitable for practical engineering applications.

It is well known that wideband beamforming can be generally categorized into two main parts: space-time beamforming and subband beamforming. Subband beamforming algorithms mainly include two substeps: substep decomposes the received wideband signal into multiple frequency bins and substep employs the narrowband beamforming techniques at each frequency bin. Therefore, the computational complexity of the proposed subband beamformer consists of two main parts: 1) the computational complexity of wideband decomposition operation and 2) the computational complexity of the proposed narrowband beamformer. The fast Fourier transform (FFT) is used to divide the wideband signal into multiple subband signals, which takes approximately $NL_3(P\log(P))$ flops. Here, let the size of sliding window be P with 50% overlapping rate, which may be most commonly used; then, the number of frames is $L_3 = \lfloor(2L)/(P) - 1\rfloor$. It is noteworthy that the overlapping rate cannot be too large; otherwise, there will be excessive redundancy between the two adjacent frames. The proposed narrowband beamformer is exploited for each frequency bin, which takes approximately $5(L_3+1)^3/3 + (L_3+1)^2N$ flops. Also, the wideband received data are processed by FFT, which are conjugate-symmetric. Thus, we only need to process the first $P/2$ data. Therefore, the overall computational complexity is about $NL_3(P\log(P)) + 5P(L_3+1)^3/6 + P(L_3+1)^2N/2$ flops.

It can be seen from the Appendix that we need to convert the received data into space-time data matrix. Suppose that the overlapping rate of two adjacent frames is 50%. Hence, the size of space-time data matrix is $(NP) \times (L_3)$. Constructing the Gram matrix of space-time data requires $(NP)(L_3)^2$ flops. Since the Gram matrix of space-time data only needs to calculate one time, the overall computational complexity of the proposed space-time beamformer is approximately equal to $5P(L_3+1)^3/3 + (L_3+1)^2(NP) + 4L_3(NP)$ flops.

The computational complexity of FCM [54] is at least $2(NP)^3/3$ flops (that is just the computational complexity of space-time covariance matrix inversion and other terms are omitted in this case). NP is much larger than $L_3 = \lfloor(2L)/(P) - 1\rfloor$. Hence, we know that the proposed algorithm equips lower computational complexity in practical applications.

F. Analysis of Adaptive Algorithm Based on Loading Technique

Through EVD of the Gram matrix, the alternative form of (15) is given by the following equation:

$$\widehat{\mathbf{R}} = \sum_{l=1}^{L} \sigma_l \mathbf{v}_l \mathbf{v}_l^H \tag{27}$$

where $\mathbf{V} = [\mathbf{v}_1, \mathbf{v}_2, \ldots, \mathbf{v}_L]$ denotes the eigenvector matrix of $\widehat{\mathbf{R}}$ and $\Sigma = \mathrm{diag}(\sigma_1, \sigma_2, \ldots, \sigma_L)$ denotes the eigenvalue

matrix of $\widehat{\mathbf{R}}$. Similarly, we can get the alternative expression of $\tilde{\mathbf{R}}$ as follows:

$$\tilde{\mathbf{R}} = \alpha \mathbf{I}_L + \kappa \widehat{\mathbf{R}} = \sum_{l=1}^{L} \frac{(\kappa\sigma_l + \alpha)}{\sigma_l} \sigma_l \mathbf{v}_l \mathbf{v}_l^H. \tag{28}$$

It can be seen from (27) and (28) that all the low-dimensional matrices of the two beamformers have a similar form. Hence, we can get a more generalized form of these low-dimensional matrices as follows:

$$\sum_{l=1}^{L} f(\sigma_l)\, \sigma_l \mathbf{v}_l \mathbf{v}_l^H \tag{29}$$

where $f(\sigma_l), l = 1, 2, \ldots, L$, is called the filter coefficient of the corresponding regularization approach.

According to the eigenvalues of the Gram matrix, we can reasonably divide the eigenvectors into two parts: the low-frequency components corresponding to the larger eigenvalues of the Gram matrix and the high-frequency components corresponding to the smaller eigenvalues of the Gram matrix. Obviously, the high-frequency components are related to the random complex noise and the low-frequency components are associated with interferences. However, the inversion of the Gram matrix is dominated by the high-frequency components. Hence, this will cause uncertainty in the linear combination vector. To deal with this issue, a suitable regularization technique should be used to filter out the high-frequency components of the inversion of the Gram matrix. Clearly, the regularization technique adopted is equivalent to a low-pass filter. Hence, the proposed algorithms can achieve better performance.

It can be seen from (29) that $f(\sigma_l), l = 1, 2, \ldots, L$, of the proposed-MVDR beamformer is equal to 1. Hence, the filter of the proposed-MVDR beamformer is an all-pass filter. The high-frequency components of the Gram matrix are not filtered out at all in this case. However, the filter coefficients of the loading technique are adaptively updated according to the received data matrix. The loading technique has two significant advantages. First, the high-frequency components of the Gram matrix are adaptively suppressed in the presence of model mismatches. Second, the beamformer scans the integral angle grid rapidly, as the loading factor is fixed when the presumed SSV varies.

It is easily seen that there are two errors in the linear combination vector: the perturbation error and the regularization error. Moreover, there is a balance between the perturbation error and the regularization error of the new beamformer. Overall, the proposed beamformer is highly efficient; hence, it is well suited for modern array systems.

IV. Simulation Results

In the first three simulations, we assume a ULA of 500 omnidirectional sensors spaced half a wavelength apart. Furthermore, 100 Monte Carlo trials are performed to obtain each point of the performance curves. The interference-to-noise ratio (INR) is specified as 30 dB. The desired signal impinges on the ULA from 0°, where the direction perpendicular to the ULA is taken as 0°. Furthermore, the six far-field point interferences arrive at the array from 2.2°, 1.5°, 0.8°, −0.6°, −1.2°, and −2.5°. The experimental results of the ATL [43], LSMI [30], WCPO-based beamformer [17], CMR-based beamformer [50], and optimal beamformer are shown in the following figures. We suppose that the angular grids of the six interferences and the SOI are set to [−2.9°, −2.1°], [−1.6°, −0.8°], [−1.0°, −0.2°], [0.4°, 1.2°], [1.1°, 1.9°], [1.8°, 2.6°], and [−0.4°, 0.4°]. All these seven angular sectors are uniformly divided into discrete sectors with the same angular interval $\Delta\theta = 0.4°$ for the CMR-based beamformer. Let the uncertainty set parameter $\varepsilon = 5$ [17].

All experiments are carried out in MATLAB v.2016b on a PC with a Windows 10 system and a 3.71-GHz CPU.

The loading factor of the ATL beamformer is given by the following equation:

$$l_{\mathrm{ATL}} = \left(\bar{\mathbf{a}}\left(\bar{\theta}_{\bar{k}}\right)^H \hat{\mathbf{R}} \bar{a}\left(\bar{\theta}_{\bar{k}}\right)\right) \Big/ \left\|\bar{\mathbf{a}}\left(\bar{\theta}_{\bar{k}}\right)\right\| \tag{30}$$

with

$$\bar{\mathbf{a}}\left(\bar{\theta}_{\bar{k}}\right) = \mathbf{a}\left(\bar{\theta}_{\bar{k}}\right) \odot \mathbf{w}_{\mathrm{DC}} \tag{31}$$

where $\mathbf{w}_{DC}$ is the Dolph–Chebyshev weight vector. The loading parameter of LSMI [30] is defined as follows:

$$l_{\mathrm{LSMI}} = \sqrt{\hat{\sigma}_M \hat{\sigma}_{M+1}} \tag{32}$$

where $\hat{\sigma}_M$ is the Mth eigenvalue (arranged in descending order) of the SCM. Specifically, $\hat{\sigma}_M$ is the minimum power of interference and $\hat{\sigma}_{M+1}$ is the maximum power of noise when the desired signal component is not present in the SCM. It can be seen that the LSMI needs some user-defined parameters, for instance, the number of interferences.

The performance of the beamformer is measured by the average value of the output SINR, which is formulated as follows:

$$\mathrm{SINR} = \frac{1}{\bar{N}} \sum_{\bar{n}=1}^{\bar{N}} \left(\sigma_{\mathbf{s}}^2 |\mathbf{w}_{\bar{n}}^H \mathbf{a}|^2\right) \Big/ \left(\mathbf{w}_{\bar{n}}^H \mathbf{R}_{i+n} \mathbf{w}_{\bar{n}}\right) \tag{33}$$

where $\bar{N}$ denotes the number of Monte Carlo runs and $\mathbf{w}_{\bar{n}}$ denotes the specified beamformer weight vector.

A. Precisely Known SSV

We consider the case [17], in which the spatial signature of the experiment is known precisely.

Fig. 2 shows the output SINR of the algorithms versus the input SNR when the number of snapshots is fixed at 50. Fig. 3 shows the average output SINR versus the number of training snapshots when the input SNR is specified as −5 dB. The beam patterns of the beamformers are shown in Fig. 4 when the number of snapshots is fixed at 50 and the input SNR is equal to −5 dB.

Fig. 2 shows that the LSMI and the proposed-LT algorithms are better than the CMR, ATL, proposed-MVDR, and WCPO beamformers, achieving superior performance that is slightly lower than the optimal SINR for all the input SNR regions. Obviously, the SMI beamformer is invalid, as the SCM is a singular matrix for a small number of samples. The computational complexity of the WCPO and CMR beamformers is greater

than that of the proposed and LSMI beamformers for LSAs. The size of the uncertainty set is not easily determined in most cases, and repeated optimization is required to calculate the loading factor of the algorithm. In the low input SNR region, the performance of the beamformer is dependent on its noise suppression ability. The diagonal loading technique employs the identity matrix, which is equipped with identical diagonal elements multiplied by a parameter to improve the array covariance matrix. However, the ATL beamformer uses a tridiagonal matrix, which has different eigenvalues, to enhance the SCM. The small eigenvalues only related to noise are uniformly suppressed by the diagonal loading technique under complex Gaussian noise. However, the high-frequency components of the SCM are nonuniformly filtered under the same circumstances. Consequently, these residual high-frequency components strongly affect the performance of the ATL beamformer under complex Gaussian noise. Therefore, poor loading matrices of the algorithm degrade its performance in the low input SNR region.

Fig. 4 shows that the beam patterns of the ATL and new beamformers have nulls in the directions of the interferences. Furthermore, the sidelobes of the proposed-LT algorithm are lower than those of the ATL beamformer. Because of the suitable loading level, the robustness of the new algorithm is superior to that of the ATL beamformer in the low input SNR region.

B. SSV Mismatch

Here, we consider the following frequently encounter errors (mismatches): direction of arrival (DOA) mismatch, amplitude (gain) and phase error, location perturbations, and coherent local scattering

$$(1+\Delta g_m)\, e^{j\Delta\phi_m} e^{j(2\pi/\bar{\lambda})(md+\Delta z_m)\cos(\theta+\Delta\theta)}. \tag{34}$$

Here, j is the imaginary unit, $\bar{\lambda}$ denotes the wavelength of the signal wavefront, d is the adjacent element spacing, $\Delta\theta$ represents the DOA error, Δg_m is the sensor gain mismatch, $\Delta\varphi_m$ represents the phase mismatch, and Δz_m is the sensor location perturbation.

The sensor gains and phase errors exist in the case of a real spatial signature. In array signal processing, we often assume that random variables, such as sensor gain, are normally distributed with a standard deviation of 0.01. Furthermore, the sensor phase errors are independent and uniformly distributed in $[-10°, 10°]$.

In the DOA mismatch case, we suppose that the assumed and real SSV are plane waves impinging the array system from 0° and 0.1°, respectively. Therefore, 0.1° mismatch is present in the SSV [1], [17], [43].

In the location perturbation case, the independent and identically distributed normal random variables Δz_m equip with 0 mean and $0.05\bar{\lambda}$ standard deviation.

Also, we assume the presumed signal travel along a single path to the array from 0°. However, the actual spatial signature is formed by five coherent local paths [17].

Figs. 5, 7, 9, and 11 show the output SINR of six beamformers versus the input SNR in the SSV mismatch case. Figs. 6, 8, 10, and 12 show the output SINR versus the number of snapshots, where the input SNR is specified as −5 dB. Compared with the simulation results shown in Figs. 2 and 3, we know that the performances of the ATL, WCPO, and CMR beamformers are degraded in the mismatch case. The uncertainty set is the prior knowledge of the WCPO beamformer. However, the WCPO beamformer involves repeated optimization to calculate the loading factor without sufficiently considering the mismatch. In other words, the uncertainty set of WCPO is accurate when a mismatch occurs in the real signal signature. When a large error is present in the received samples or the SSV, the performance of the WCPO beamformer is severely degraded, as is the case with the ATL beamforming algorithm.

There is a mismatch between the real signal signature and the presumed one; in this case, the desired signal of the array covariance matrix will be regarded as interference and canceled. The model errors result in signal cancellation, which causes performance degradation of many excellent adaptive beamformers in the high input SNR region. Hence, the signal cancellation phenomenon of the ATL and WCPO beamformers

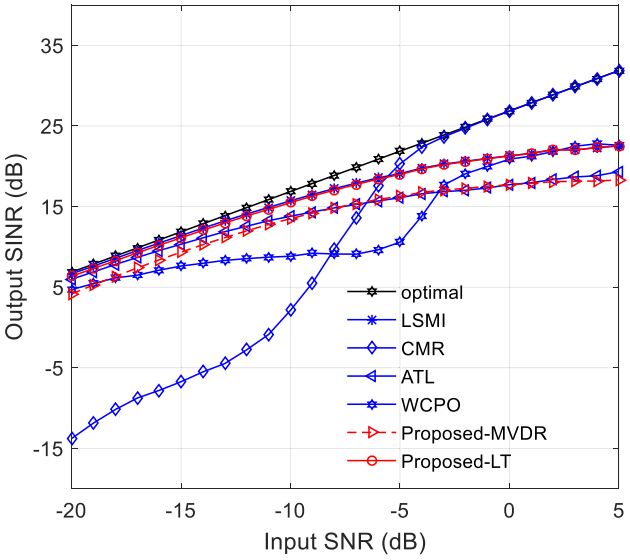

Fig. 2. Output SINR versus input SNR (exactly known SSV).

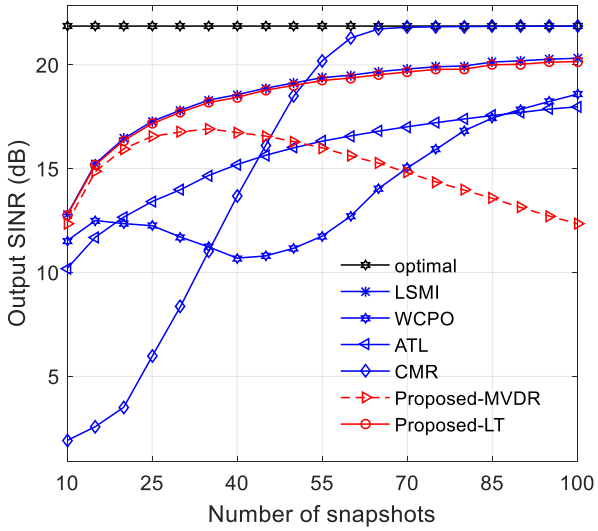

Fig. 3. Output SINR versus number of snapshots (exactly known SSV).

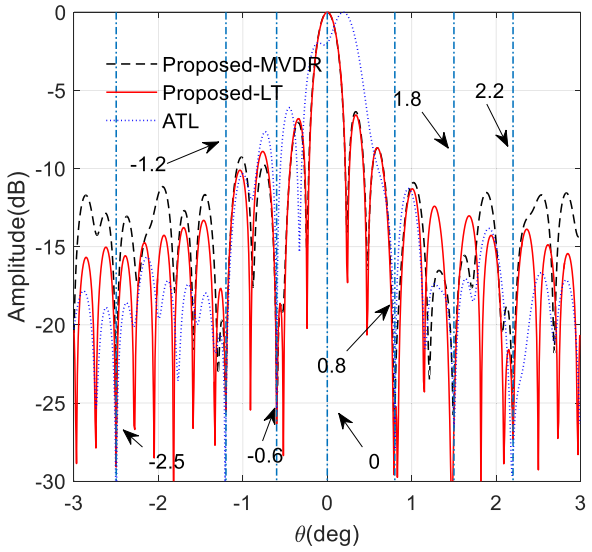

Fig. 4. Beam patterns (exactly known SSV).

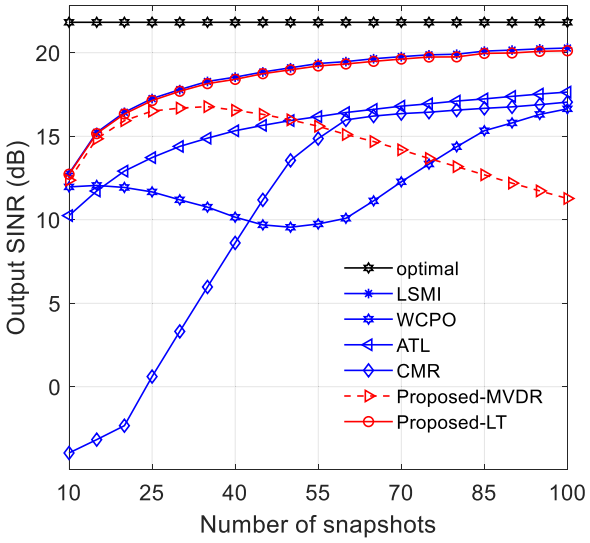

Fig. 6. Output SINR versus the number of snapshots (amplitude and phase error).

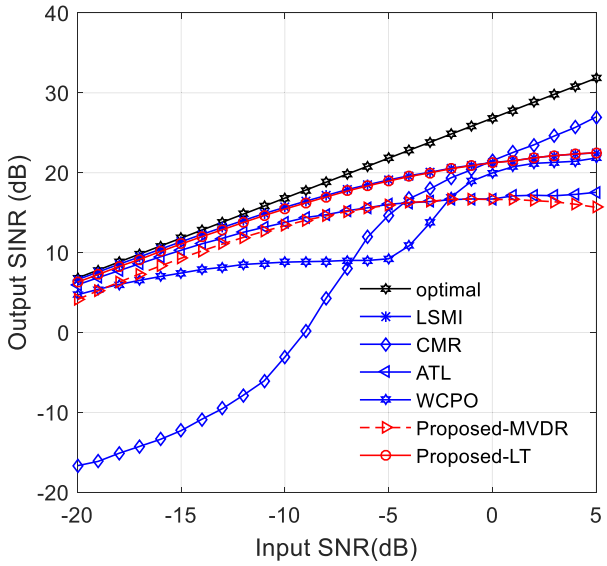

Fig. 5. Output SINR versus input SNR (amplitude and phase error).

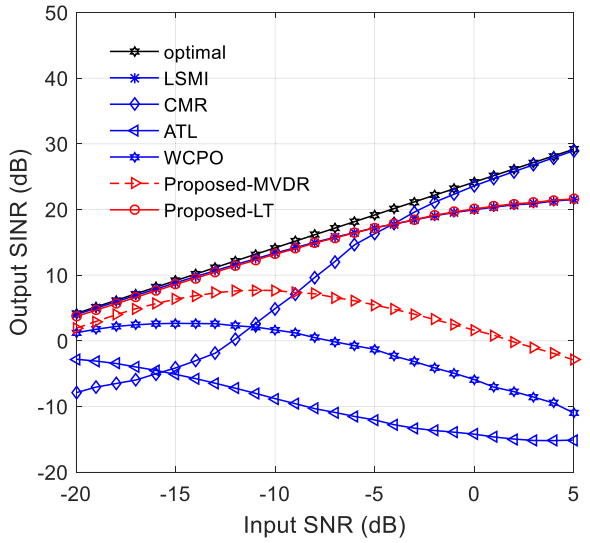

Fig. 7. Output SINR versus input SNR (DOA mismatch).

is more prominent than that of the proposed-LT beamformer in the mismatch case.

C. Computational Complexity

This section quantitatively compares the computational complexities of the new algorithm and existing algorithms in terms of computational time. Also, other compared schemes use the same number of snapshots as the proposed scheme. The number of sensors is set to 1000 in this experiment.

The definition of computational time is given by the following equation:

$$10 \log 10 \left(T_1 \right) \tag{35}$$

where T_1 is the averaged elapsed time of a beamforming algorithm in the scanning mode.

Fig. 13 shows the computational time versus the number of snapshots where both $\bar{K}$ and $\hat{K}$ are equal to 1. Fig. 14 shows the computational time versus the number of snapshots where $\bar{K}$ is fixed at 20 and $\hat{K}$ is set to 360. Furthermore, Fig. 14 corresponds to the case where the beamformers work in the "beamforming mode." This means that the angle sectors of the interferences and SOI are obtained using some angle estimation techniques by the CMR beamformer. And so, even more, is LSMI. However, prior knowledge (angle sectors of interferences and desired signal) is required by a beamformer in the scanning mode. Hence, the CMR beamformers are unable to work in the scanning mode. Moreover, the performance (SINR) of CMR is strongly dependent on the accuracies of the angle sectors and the size of the angular interval. A smaller angular interval results in a higher SINR. However, the computational time of the CMR beamformer increases as the angular interval improves. Clearly, the proposed algorithm achieves better performance than the reference algorithms. Hence, it is perfect for the online scanning mode. Obviously, the computational time of the proposed algorithm is less than

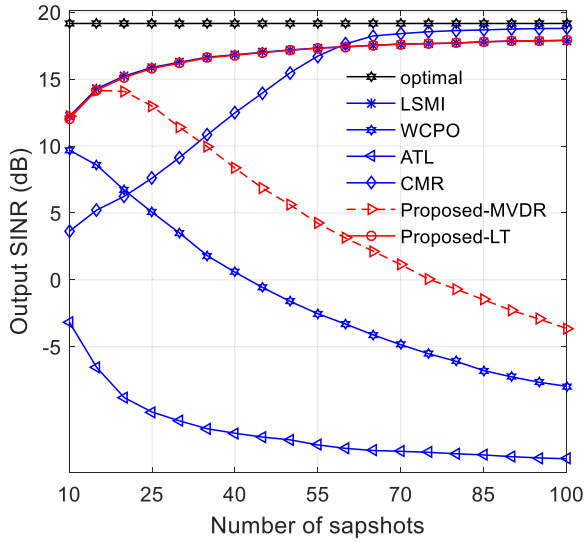

Fig. 8. Output SINR versus the number of snapshots (DOA mismatch).

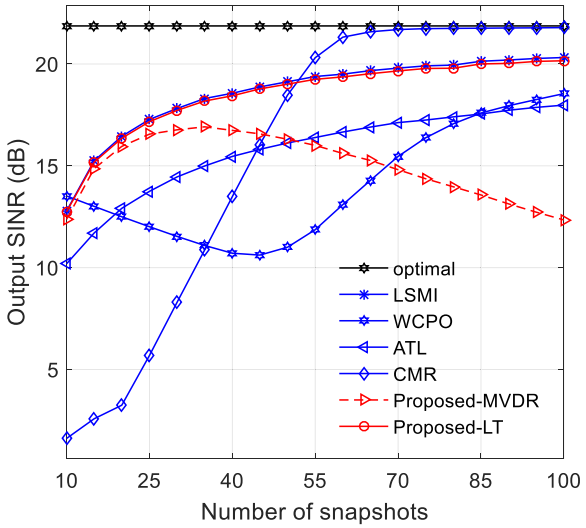

Fig. 10. Output SINR versus the number of snapshots (location perturbation).

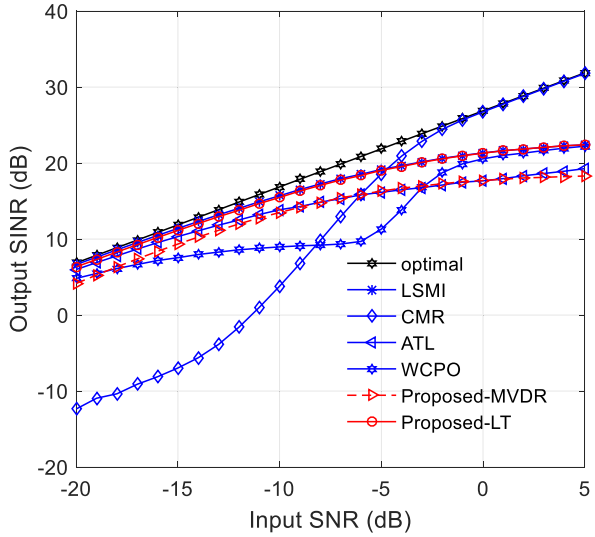

Fig. 9. Output SINR versus input SNR (location perturbation).

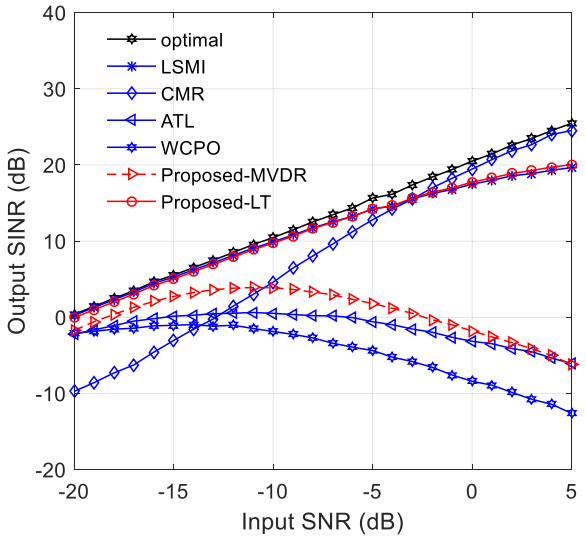

Fig. 11. Output SINR versus input SNR (coherent local scattering).

that of the LSMI, WCPO, CMR, and ATL beamformers for a small number of samples.

D. Space-Time Beamforming

Our simulation scenario comprises the following setup: the number N of ULA antennas is set as 50; the interelement spacing of the half wavelength of the highest frequency; the number of space-time delay time-lines is 30 (Frost filter); the number of snapshots used to build the beampattern is 200; one broadband SOI comes from $-10°$ and one broadband interference signal is from $-30°$; the lowest frequencies of the two signals are 0.9 GHz; the frequency bands of the two signals are 200 MHz, the pulsewidths of two signals (multifrequency superimposed signal) are set as 10 μs; the sampling frequency is reasonably chosen as 2.5 GHz; the SNR and INR are assumed as 0 and 30 dB, respectively; and the number of Monte Carlo trials per point of the performance curves is 1000. Also, the beampattern of [54], which is also called the frequency constraint method (FCM), shows in the experiment.

In Fig. 15, the beampatterns of the proposed space-time beamforming algorithm are provided. As shown in Fig. 15(a)–(c), the proposed algorithm applied in the Frost structures exhibits an undistorted response to the SOI and efficiently restrained nulls for the interferences. All the results indicate that the new algorithm preserves a satisfactory performance on beam patterns. Specifically, as shown in Fig. 15(b), the main lobe direction is located at $-10°$, which is the DOA of the SOI. Therefore, the proposed algorithm can efficiently enhance the SOI and detect targets. Also, the null of the beampattern is located at $-30°$. Hence, the new algorithm can significantly suppress interferences and noise.

Fig. 16 shows the beampattern of FCM, where the number of snapshots is fixed at 50. It can be seen from Figs. 15(b) and 16(b) that the complex beam squint effects appear in Fig. 16. If the SOI impinges on the array from 0°,

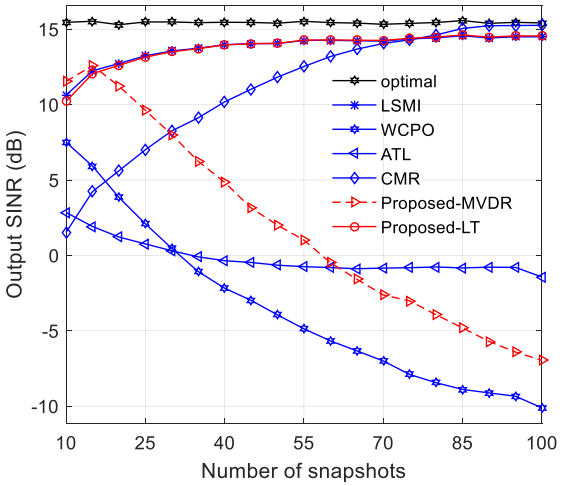

Fig. 12. Output SINR versus the number of snapshots (coherent local scattering).

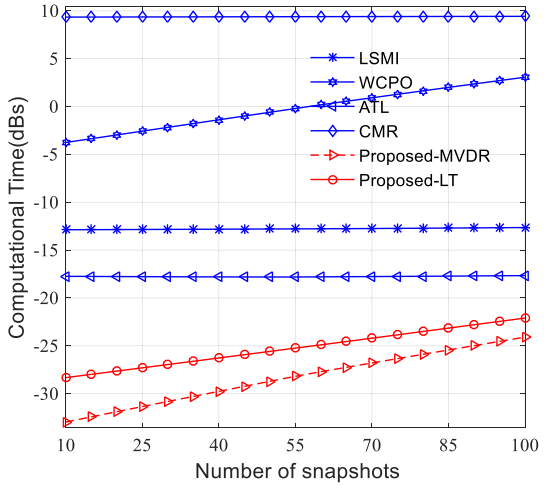

Fig. 13. Computational time of algorithms versus number of samples, where both $\bar{K}$ and $\hat{K}$ are equal to 1.

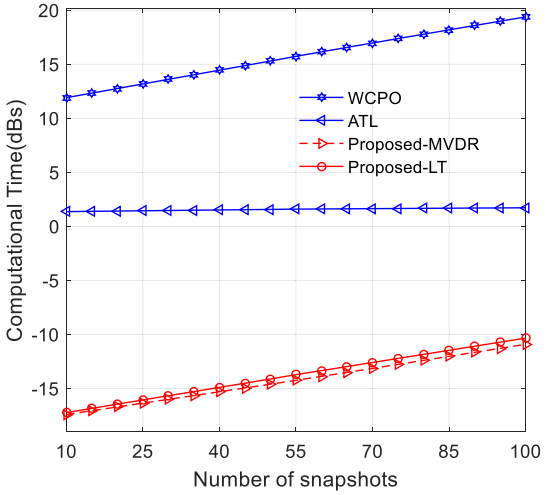

Fig. 14. Computational time of algorithms versus the number of samples, where $\bar{K}$ is fixed at 20 and $\hat{K}$ is set to 360 (third example).

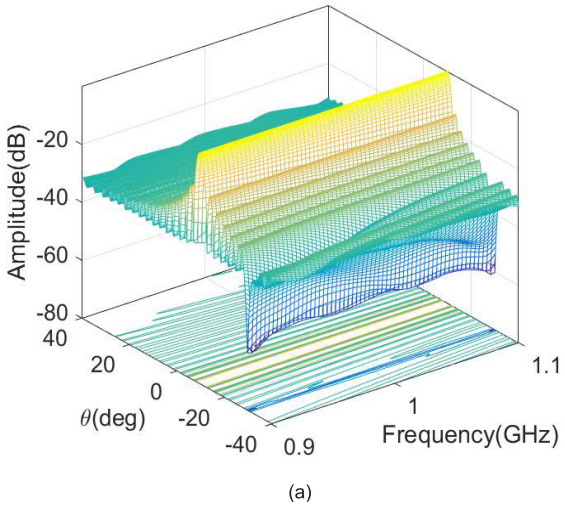

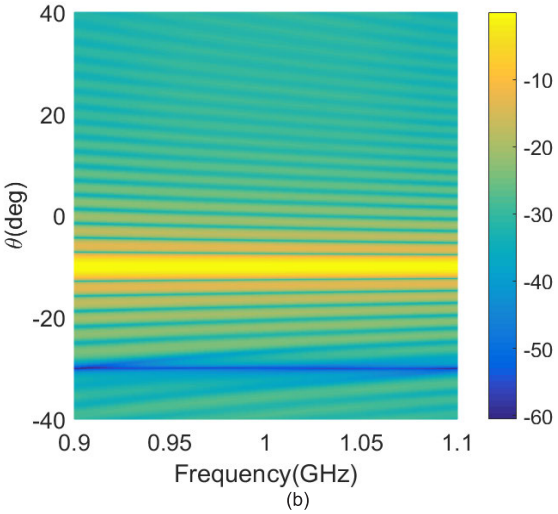

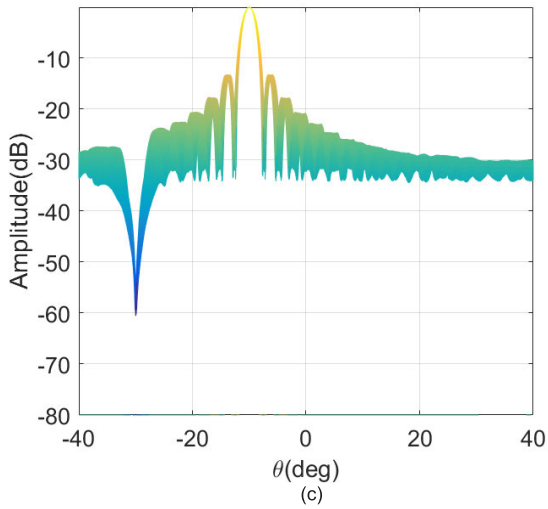

Fig. 15. Beampatterns of the proposed algorithm (space-time beamforming). (a) Wireframe of proposed space-time beamformer. (b) Vertical view of the proposed space-time beamformer. (c) Horizontal view of the proposed space-time beamformer.

then there is no beam squint. As the DOA of SOI is increased, the beam squint of Fig. 16 becomes serious. The main reason is that when the presumed frequency in the frequency constrain matrix is different from that of the received signal, then the beam squint is present in the beam pattern. In other words, the frequency mismatch leads to a DOA error. It is worth noting that the beam squint is not linear and is very difficult

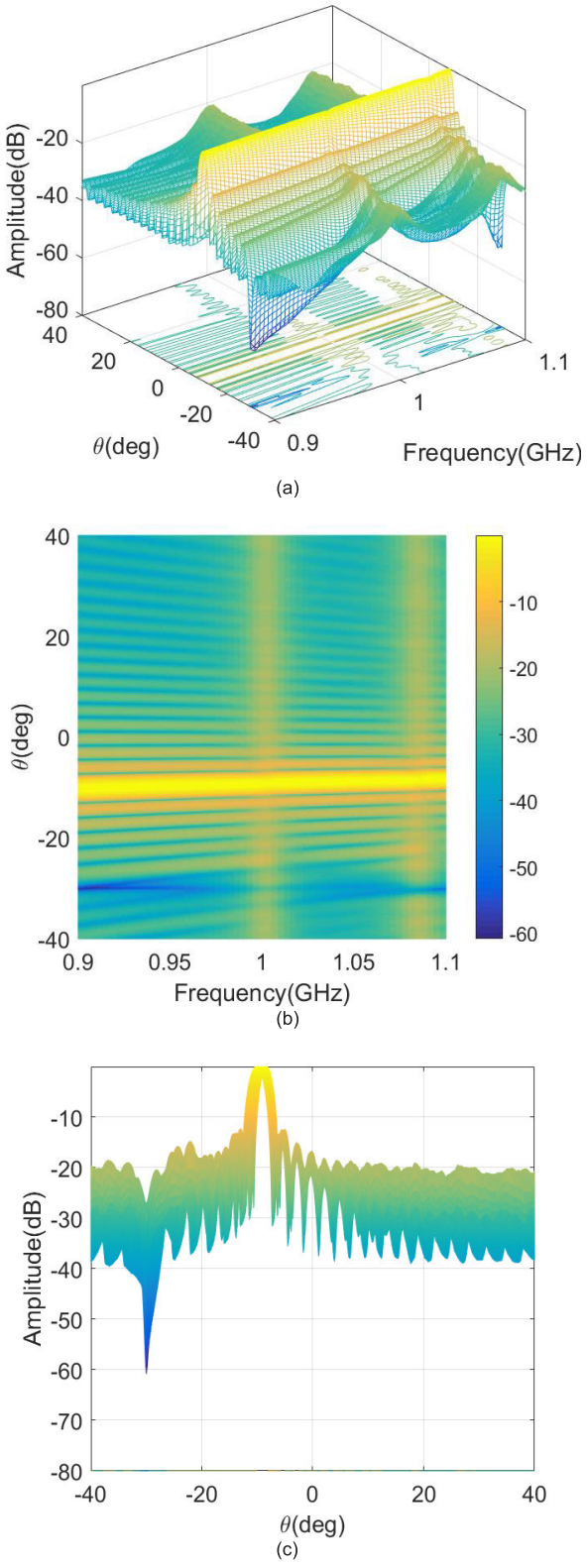

Fig. 16. Beampatterns of FCM algorithm (space-time beamforming). (a) Wireframe of FCM space-time beamformer. (b) Vertical view of FCM space-time beamformer. (c) Vertical view of FCM space-time beamformer.

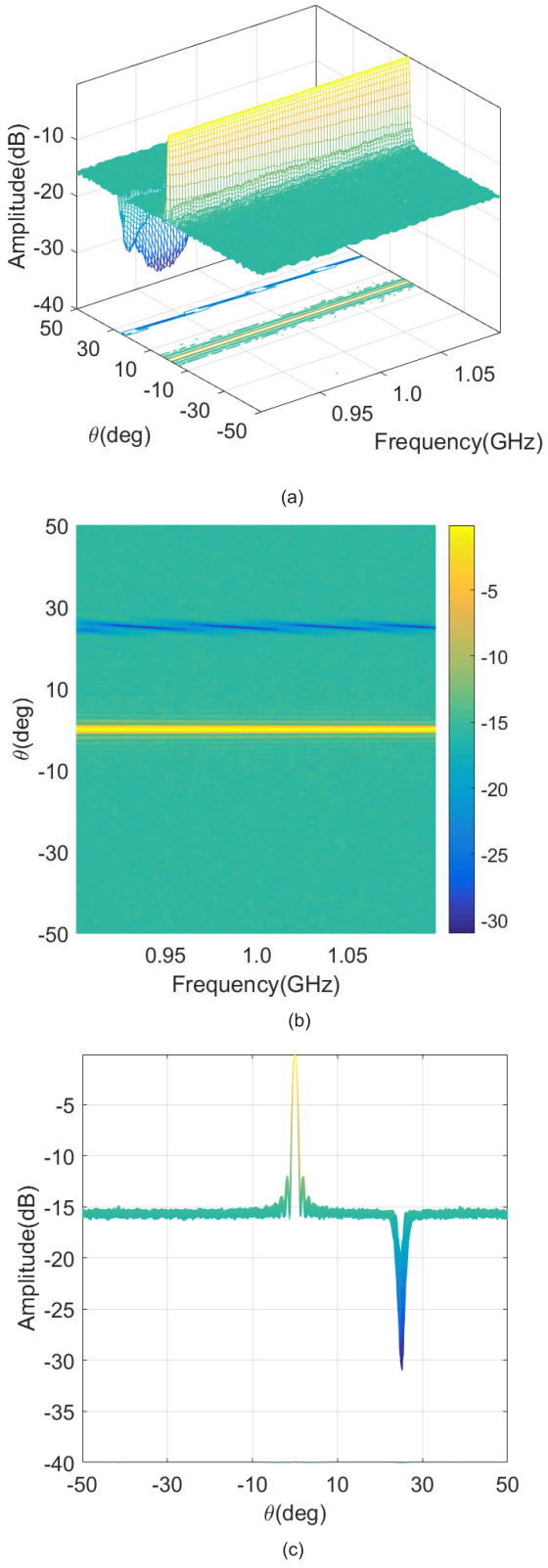

Fig. 17. Beampatterns of the proposed algorithm (subband beamforming). (a) Wireframe of subband beamformer. (b) Vertical view of the proposed subband beamformer. (c) Horizontal view of the proposed subband beamformer.

to be corrected. In addition, if there is a DOA mismatch between the frequency constraint matrix and the received signal, the main lobe of the beam pattern will be shifted in the angular domain, and the magnitude of the shift is equal to the mismatch size. It is true that while dealing with large arrays, beam squint is very common. We can clearly see that the

beam squint does not present in Fig. 15(b) since there is not any mismatch. It is worthwhile to decrease the beam squint effects by increasing the number of frequency bins and the number of angular grids. Interestingly, at the cost of memory consumption, the space-time weight vector of each frequency bin can be obtained by parallel computing. Thus, compared with FCM, the proposed space-time beamformer equips with low computational complexity because it uses small samples.

E. Subband Beamforming

In this experiment, the number of sensors is 100; the frequency range is [0.91.1] GHz; one interference and SOI impinge on the array from 0° and 25° (both of them are chirp signals with 10-μs impulse width), respectively; and the number of snapshots of each frame is 1024 (two adjacent frames without overlap). At the same time, there is a Hanning window that is imposed on every frame. The number of Monte Carlos trials per point of the performance curves is 1000.

Fig. 17 shows the beampatterns and their different (vertical and horizontal) views from the proposed approaches. Also, the interval of angle is 0.1°. It can be seen from Fig. 17 that the new algorithm yields a satisfactory beam pattern shape.

V. Conclusion

This study formulated a new type of beamformer weight vector. This formulation is based on the fact that the received data matrix consists of interferences and the expected signal, and the optimal weight vector is linearly represented by the basis vectors of the signal-plus-interference subspace. Using the kernel method and shrinkage technique, we proposed an adaptive beamforming algorithm, with advantages such as a high convergence rate and low computational complexity. Also, the loading factor method does not require user-defined parameters, such as the number of interferences and the level of noise. The simulation results show that the proposed algorithms exhibit superior output SINR for a small number of samples. Furthermore, the extensive analysis demonstrated that the calculation cost of the proposed-LT algorithm is much lower than that of the WCPO, CMR, classical LSMI, and ATL beamformers.

In real applications, since the dimension of the frequency constraint matrix and space-time data matrix is very high, conventional space-time beamformers in the large sample case may take the huge computational complexity. Thus, these space-time beamformers are difficult to be applied in practical engineering. Fortunately, the proposed algorithm equips with a lower computational load and a good performance in the case of the small samples.

Appendix

In small samples case, space-time beamforming is constructed by the following optimization problem:

$$\underset{\mathbf{W}}{\text{minimize}} \quad \text{trace}\left\{\mathbf{W}^H\left(\mathbf{X}_1\mathbf{X}_1^H/L_3\right)\mathbf{W}\right\} \tag{36}$$

$$\text{subject to} \quad \mathbf{C}_F^H(\theta)\,\mathbf{W} = \text{diag}\,(\mathbf{f}_d)\,, \tag{37}$$

$$\mathbf{W} = [\mathbf{C}_F(\theta)\,, \mathbf{X}_1]\,\mathbf{B} \in \mathbb{C}^{NP\times P} \tag{38}$$

where $\mathbf{f}_d = [e^{-j2\pi f_1(Q-1)T_s}, \ldots, e^{-j2\pi f_J(Q-1)T_s}] \in \mathbb{C}^{1\times P}\mathbf{B} \in \mathbb{C}^{(P+L_3)\times P}$ $\mathbf{C}_F(\theta) = [\mathbf{c}_F(\theta, f_1), \mathbf{c}_F(\theta, f_2), \ldots, \mathbf{c}_F(\theta, f_J)] \in \mathbb{C}^{NP\times P}\mathbf{c}_F(\theta, f_i) = \mathbf{c}_{T_s}(\theta, f_i) \otimes \mathbf{c}_\tau(f_i) \in \mathbb{C}^{NP\times 1}$, $\mathbf{c}_{T_s}(f_i) = [1, \ldots, e^{-j2\pi f_i(Q-1)T_s}]^T \in \mathbb{C}^{P\times 1}$, $\mathbf{c}_\tau(\theta, f_i) = [e^{-j2\pi f_i\tau_1(\theta)}, e^{-j2\pi f_i\tau_2(\theta)} \cdots, e^{-j2\pi f_i\tau_N(\theta)}]^{\mathrm{T}} \in \mathbb{C}^{N\times 1}$, P is the number of time delay lines, T_s denotes the sampling interval, $\tau_n = [(n-1)d\sin(\theta)]/c$, d represents the spacing of adjacent sensors, $c$is the signal speed, $\mathbf{x}_1(n) = [\mathbf{x}(n); \mathbf{x}(n+1); \cdots; \mathbf{x}(n+P-1)]$ is the space-time data vector, and $\mathbf{X}_1 = [\mathbf{x}_1(1), \ldots, \mathbf{x}_1(L_3)]$ denotes the space-time data matrix in which L_2 is the number of space-time samples.

Let $\mathbf{R}_4 = [\mathbf{R}_3, \mathbf{R}_2]^H[\mathbf{R}_3, \mathbf{R}_2]/L_3$, $\mathbf{C}_2 = \mathbf{C}_F^H\mathbf{C}_F$, $\mathbf{R}_2 = \mathbf{X}_1^H\mathbf{X}_1$, $\mathbf{R}_3 = \mathbf{X}_1^H\mathbf{C}_F(\theta)$, and $\mathbf{R}_5 = [\mathbf{C}_2, \mathbf{R}_3^H]$. Hence, (36)–(38) are rewritten as follows:

$$\begin{cases} \underset{\mathbf{B}}{\text{minimize}} & \text{tr}\left(\mathbf{B}^H\mathbf{R}_4\mathbf{B}\right) \\ \text{subject to} & \mathbf{R}_5\mathbf{B} = \text{diag}\,(\mathbf{f}_d)\,. \end{cases} \tag{39}$$

By employing the Lagrange multiplier method, we convert (36) into an unconstrained one. Hence, we get the following optimization expression:

$$\underset{\mathbf{B}}{\text{minimize}}\, J = \text{trace}\left\{\mathbf{B}^H\mathbf{R}_4\mathbf{B} + (\text{diag}\,(\mathbf{f}_d) - \mathbf{R}_5\mathbf{B})^H\,\mathbf{\Gamma}\right\} \tag{40}$$

where $\mathbf{\Gamma}$ is the Lagrange multiplier matrix. Then, we have

$$\mathbf{B} = \mathbf{R}_4^{-1}\mathbf{R}_5^H\mathbf{\Gamma}. \tag{41}$$

Inserting (41) into (36), we get

$$\mathbf{\Gamma} = \left(\mathbf{R}_5\mathbf{R}_4^{-1}\mathbf{R}_5^H\right)^{-1}\text{diag}\,(\mathbf{f}_d)\,. \tag{42}$$

Combining (38), (41), and (42) yields

$$\mathbf{W} = [\mathbf{C}_F, \mathbf{X}_1]\,\mathbf{R}_4^{-1}\mathbf{R}_5^H\left(\mathbf{R}_5\mathbf{R}_4^{-1}\mathbf{R}_5^H\right)^{-1}\text{diag}\,(\mathbf{f}_d)\,. \tag{43}$$

References

[1] X.-J. Zhang, H. Xie, D.-Z. Feng, W. X. Zheng, and H. S. Hu, "Fast and robust adaptive beamforming algorithms for large-scale arrays with small samples," *Signal Process.*, vol. 188, Nov. 2021, Art. no. 108223.

[2] P. Stoica, J. Li, X. Zhu, and J. R. Guerci, "On using a priori knowledge in space-time adaptive processing," *IEEE Trans. Signal Process.*, vol. 56, no. 6, pp. 2598–2602, Jun. 2008.

[3] S. M. Ellison, S. R. Mghabghab, and J. A. Nanzer, "Multi-node open-loop distributed beamforming based on scalable, high-accuracy ranging," *IEEE Sensors J.*, vol. 22, no. 2, pp. 1629–1637, Jan. 2022, doi: 10.1109/JSEN.2021.3130793.

[4] A. B. Gershman, E. Nemeth, and J. F. Bohme, "Experimental performance of adaptive beamforming in a sonar environment with a towed array and moving interfering sources," *IEEE Trans. Signal Process.*, vol. 48, no. 1, pp. 246–250, Jan. 2000.

[5] M. Cremer, U. Dettmar, C. Hudasch, R. Kronberger, R. Lerche, and A. Pervez, "Localization of passive UHF RFID tags using the AoAct transmitter beamforming technique," *IEEE Sensors J.*, vol. 16, no. 6, pp. 1762–1771, Mar. 2016, doi: 10.1109/JSEN.2015.2503640.

[6] G. W. Kant, P. D. Patel, S. J. Wijnholds, M. Ruiter, and E. Van Der Wal, "EMBRACE: A multi-beam 20,000-element radio astronomical phased array antenna demonstrator," *IEEE Trans. Antennas Propag.*, vol. 59, no. 6, pp. 1990–2003, Jun. 2011.

[7] M. A. Vázquez, L. Blanco, and A. I. Pérez-Neira, "Spectrum sharing backhaul satellite-terrestrial systems via analog beamforming," *IEEE J. Sel. Topics Signal Process.*, vol. 12, no. 2, pp. 270–281, May 2018, doi: 10.1109/JSTSP.2018.2824980.

[8] S. D. Somasundaram, A. Jakobsson, and N. H. Parsons, "Robust and automatic data-adaptive beamforming for multidimensional arrays," *IEEE Trans. Geosci. Remote Sens.*, vol. 50, no. 11, pp. 4642–4656, Nov. 2012.

[9] J. Choi, "Opportunistic beamforming with single beamforming matrix for virtual antenna arrays," *IEEE Trans. Veh. Technol.*, vol. 60, no. 3, pp. 872–881, Mar. 2011.

[10] X. Wang, Z. Lin, F. Lin, and L. Hanzo, "Joint hybrid 3D beamforming relying on sensor-based training for reconfigurable intelligent surface aided TeraHertz-based multiuser massive MIMO systems," *IEEE Sensors J.*, vol. 22, no. 14, pp. 14540–14552, Jul. 2022, doi: 10.1109/JSEN.2022.3182881.

[11] C. Xiang, D.-Z. Feng, H. Lv, J. He, and Y. Cao, "Robust adaptive beamforming for MIMO radar," *Signal Process.*, vol. 90, no. 12, pp. 3185–3196, Dec. 2010.

[12] Z. Ding and J. Xie, "Joint transmit and receive beamforming for cognitive FDA-MIMO radar with moving target," *IEEE Sensors J.*, vol. 21, no. 18, pp. 20878–20885, Sep. 2021, doi: 10.1109/JSEN.2021.3100332.

[13] H. Huang, Y. Peng, J. Yang, W. Xia, and G. Gui, "Fast beamforming design via deep learning," *IEEE Trans. Veh. Technol.*, vol. 69, no. 1, pp. 1065–1069, Jan. 2020.

[14] J. Li, P. Stoica, and Z. Wang, "On robust Capon beamforming and diagonal loading," *IEEE Trans. Signal Process.*, vol. 51, no. 7, pp. 1702–1715, Jul. 2003.

[15] B. D. Carlson, "Covariance matrix estimation errors and diagonal loading in adaptive arrays," *IEEE Trans. Aerosp. Electron. Syst.*, vol. AEP-24, no. 4, pp. 397–401, Jul. 1988.

[16] Z. Xu, H. Li, and K. Yang, "A modified differential beamforming and its application for DOA estimation of low frequency underwater signal," *IEEE Sensors J.*, vol. 20, no. 16, pp. 8890–8902, Aug. 2020, doi: 10.1109/JSEN.2020.2988025.

[17] S. A. Vorobyov, A. B. Gershman, and Z.-Q. Luo, "Robust adaptive beamforming using worst-case performance optimization: A solution to the signal mismatch problem," *IEEE Trans. Signal Process.*, vol. 51, no. 2, pp. 313–324, Feb. 2003.

[18] C.-C. Lee and J.-H. Lee, "Eigenspace-based adaptive array beamforming with robust capabilities," *IEEE Trans. Antennas Propag.*, vol. 45, no. 12, pp. 1711–1716, Dec. 1997.

[19] M. Wax and T. Kailath, "Detection of signals by information theoretic criteria," *IEEE Trans. Acoust., Speech, Signal Process.*, vol. ASSP-33, no. 2, pp. 387–392, Apr. 1985.

[20] Z. Zhang, K. C. Teh, and K. H. Li, "Study of three-dimensional beamforming strategies in cellular networks with clustered user distribution," *IEEE Trans. Veh. Technol.*, vol. 65, no. 12, pp. 10208–10213, Dec. 2016.

[21] F. Rubio and X. Mestre, "Generalized consistent estimation on low-rank Krylov subspaces of arbitrarily high dimension," *IEEE Trans. Signal Process.*, vol. 57, no. 10, pp. 3787–3800, Oct. 2009.

[22] G. Farquharson, P. Lopez-Dekker, and S. J. Frasier, "Contrast-based phase calibration for remote sensing systems with digital beamforming antennas," *IEEE Trans. Geosci. Remote Sens.*, vol. 51, no. 3, pp. 1744–1754, Mar. 2013.

[23] F. Shen, F. Chen, and J. Song, "Robust adaptive beamforming based on steering vector estimation and covariance matrix reconstruction," *IEEE Commun. Lett.*, vol. 19, no. 9, pp. 1636–1639, Sep. 2015.

[24] D. A. Pados and G. N. Karystinos, "An iterative algorithm for the computation of the MVDR filter," *IEEE Trans. Signal Process.*, vol. 49, no. 2, pp. 290–300, Feb. 2001.

[25] K. Rao and I. Karlsson, "Low sidelobe design considerations of large linear array antennas with contiguous subarrays," *IEEE Trans. Antennas Propag.*, vol. AP-35, no. 4, pp. 361–366, Apr. 1987.

[26] R. L. Haupt, "Optimized weighting of uniform subarrays of unequal sizes," *IEEE Trans. Antennas Propag.*, vol. 55, no. 4, pp. 1207–1220, Apr. 2007.

[27] R. L. Haupt, "Reducing grating lobes due to subarray amplitude tapering," *IEEE Trans. Antennas Propag.*, vol. AP-33, no. 8, pp. 846–850, Aug. 1985.

[28] K. R. Müller, S. Mika, G. Rätsch, K. Tsuda, and B. Schölkopf, "An introduction to kernel-based learning algorithms," *IEEE Trans. Neural Netw.*, vol. 12, no. 2, pp. 181–201, Feb. 2001.

[29] S. Gong, C. Xing, S. Ma, Z. Zhang, and Z. Fei, "Secure wideband beamforming design for two-way MIMO relaying systems," *IEEE Trans. Veh. Technol.*, vol. 68, no. 4, pp. 3472–3486, Apr. 2019.

[30] Y. L. Kim, S. U. Pillai, and J. R. Guerci, "Optimal loading factor for minimal sample support space-time adaptive radar," in *Proc. IEEE Int. Conf. Acoust., Speech Signal Process., (ICASSP)*, May 1998, pp. 2505–2508.

[31] X. Mestre and M. A. Lagunas, "Finite sample size effect on minimum variance beamformers: Optimum diagonal loading factor for large arrays," *IEEE Trans. Signal Process.*, vol. 54, no. 1, pp. 69–82, Jan. 2006.

[32] P. Palanisamy, N. Kalyanasundaram, and P. M. Swetha, "Two-dimensional DOA estimation of coherent signals using acoustic vector sensor array," *Signal Process.*, vol. 92, no. 1, pp. 19–28, Jan. 2012.

[33] X. Mestre and M. Á. Lagunas, "Modified subspace algorithms for DoA estimation with large arrays," *IEEE Trans. Signal Process*, vol. 56, no. 2, pp. 598–614, Feb. 2008.

[34] J. Qian, Z. He, W. Zhang, Y. Huang, N. Fu, and J. Chambers, "Robust adaptive beamforming for multiple-input multiple-output radar with spatial filtering techniques," *Signal Process.*, vol. 143, pp. 152–160, Feb. 2018.

[35] F. Huang, W. Sheng, X. Ma, and W. Wang, "Robust adaptive beamforming for large-scale arrays," *Signal Process.*, vol. 90, no. 1, pp. 165–172, Jan. 2010.

[36] W. Liu, S. Weiss, J. G. McWhirter, and I. K. Proudler, "Frequency invariant beamforming for two-dimensional and three-dimensional arrays," *Signal Process.*, vol. 87, no. 11, pp. 2535–2543, Nov. 2007.

[37] T. Lv, F. Tan, H. Gao, and S. Yang, "A beamspace approach for 2-D localization of incoherently distributed sources in massive MIMO systems," *Signal Process.*, vol. 121, pp. 30–45, Apr. 2016.

[38] F. Huang, W. Sheng, C. Lu, and X. Ma, "A fast adaptive reduced rank transformation for minimum variance beamforming," *Signal Process.*, vol. 92, no. 12, pp. 2881–2887, Dec. 2012.

[39] C. Xiang, D.-Z. Feng, H. Lv, J. He, and H.-W. Liu, "Three-dimensional reduced-dimension transformation for MIMO radar space–time adaptive processing," *Signal Process.*, vol. 91, no. 8, pp. 2121–2126, Aug. 2011.

[40] D.-Z. Feng, X.-M. Li, H. Lv, H.-W. Liu, and Z. Bao, "Two-sided minimum-variance distortionless response beamformer for MIMO radar," *Signal Process.*, vol. 89, no. 3, pp. 328–332, Mar. 2009.

[41] F. Huang, W. Sheng, and X. Ma, "Modified projection approach for robust adaptive array beamforming," *Signal Process.*, vol. 92, no. 7, pp. 1758–1763, Jul. 2012.

[42] F.-G. Yan, Y. Shen, and M. Jin, "Fast DOA estimation based on a split subspace decomposition on the array covariance matrix," *Signal Process.*, vol. 115, pp. 1–8, Oct. 2015.

[43] M. Zhang, X. Chen, and A. Zhang, "A simple tridiagonal loading method for robust adaptive beamforming," *Signal Process.*, vol. 157, pp. 103–107, Apr. 2019.

[44] O. Besson, "An alternative to diagonal loading for implementation of a white noise array gain constrained robust beamformer," *Signal Process.*, vol. 152, pp. 79–82, Nov. 2018.

[45] Y. Feng, G. S. Lia, Z. W. Yang, P. Zhang, and G. S. Liao, "Robust beamforming via alternating iteratively estimating the steering vector and interference-plus-noise covariance matrix," *Digital Signal Processing*, vol. 99, pp. 1–12 2019.

[46] Y. Feng, G. Liao, J. Xu, S. Zhu, and C. Zeng, "Robust adaptive beamforming against large steering vector mismatch using multiple uncertainty sets," *Signal Process.*, vol. 152, pp. 320–330, Nov. 2018.

[47] L. N. Ribeiro, A. L. F. De Almeida, and J. C. M. Mota, "Separable linearly constrained minimum variance beamformers," *Signal Process.*, vol. 158, pp. 15–25, May 2019.

[48] Y. Liu, C. Liu, D. Hu, and Y. Zhao, "Robust adaptive beam forming against random calibration error via interference-plus-noise covariance matrix reconstruction," *Signal Process.*, vol. 158, pp. 107–115, May 2019.

[49] X. Li, D. Wang, X. Ma, and Z. Xiong, "Robust adaptive beamforming using iterative variable loaded sample matrix inverse," *Electron. Lett.*, vol. 54, no. 9, pp. 546–548, May 2018.

[50] X. Yuan and L. Gan, "Robust adaptive beamforming via a novel subspace method for interference covariance matrix reconstruction," *Signal Process.*, vol. 130, pp. 233–242, Jan. 2017.

[51] Y. Gu and A. Leshem, "Robust adaptive beamforming based on interference covariance matrix reconstruction and steering vector estimation," *IEEE Trans. Signal Process.*, vol. 60, no. 7, pp. 3881–3885, Jul. 2012.

[52] L. Huang, J. Zhang, X. Xu, and Z. Ye, "Robust adaptive beamforming with a novel interference-plus-noise covariance matrix reconstruction method," *IEEE Trans. Signal Process.*, vol. 63, no. 7, pp. 1643–1650, Apr. 2015.

[53] S. Zhang, W. Sheng, Y. Han, and X. Ma, "Generalised reduced-rank structure for broadband space–time GSC and its fast algorithm," *Signal Process.*, vol. 133, pp. 117–121, Apr. 2017.

[54] R. Ebrahimi and S. R. Seydnejad, "Elimination of pre-steering delays in space-time broadband beamforming using frequency domain constraints," *IEEE Commun. Lett.*, vol. 17, no. 4, pp. 769–772, Apr. 2013.